https://doi.org/10.5194/nhess-2022-50
Preprint. Discussion started: 11 March 2022

Natural Hazards and Earth System Sciences
Discussions

Spatio-temporal analysis of the role of climate cycles on landslide activity: the case of Majorca (Spain)

Juan Antonio Luque-Espinar[1], Rosa María Mateos[1], Roberto Sarro[2], Eduardo Peña[2], Cristina Reyes-Carmona[1], Mónica Martínez-Corbella[2]

[1]Geological and Mining Institute of Spain from the National Research Council (IGME_CSIC), Urb Alcázar del Genil, edf Zulema 4 bajo, 18006 Granada, Spain.
[2]Geological and Mining Institute of Spain from the National Research Council (IGME_CSIC), Ríos Rosas 23, 28003 Madrid, Spain.

Correspondence to: Juan A. Luque-Espinar (ja.luque@csic.es)

Abstract. Intense precipitation is one of the main drivers of landslides around the globe. On a global scale, the occurrence of very wet periods is controlled by different, well-known natural cycles: ENSO, NAO, SUNSPOT, etc. In this paper, we present a spatio-temporal analysis of climate cycles on the island of Majorca (Spain) and their correlation with the landslide inventory. Firstly, using spectral analysis techniques, the main climatic cycles that control the rainy periods on the island have been identified. For this purpose, rainfall data from 62 weather stations have been analysed in a comprehensive manner, with time series of more than 30 years. The cycles with the greatest influence on rainfall, from the point of view of statistical confidence, are ENSO (5.6y and 3.5y), as well as NAO (7.5y) and QBO. Then, using geostatistical methods, the distribution of rainfall during dry, average, and wet years was mapped, as was the spatial representation of the statistical significance of the different natural cycles, in order to define the areas of greatest danger from heavy rainfall. The Serra de Tramuntana is not only the rainiest region of the island, but also the area where the highest values of statistical confidence for the set of climatic cycles are concentrated. The 5 largest landslides of the series are very well located in the areas of highest statistical weight, mainly for the NAO (7.5 y), QBO and HALO (22.4 y) cycles, as well as in the wettest sector for the wet type year.

1 Introduction

Rainfall-related geohazards are characterised by cyclical components. (Luque-Espinar et al., 2017; Xoplaki et al., 2012). Different authors have linked climate cycles, such as ENSO or NAO, to major natural disasters in different parts of the world, including the Mediterranean area. (Luque-Espinar et al., 2008; Muñoz-Díaz and Rodrigo, 2005; Rodó et al., 1997; Tramblay et al., 2013; Xoplaki et al., 2012).

Among the different climatic cycles that have visible effects on a human scale, the following should be highlighted:

- Quasi-Biennial Oscillation (QBO): 2 and 2.9 years (Labitzke et al., 1990).

https://doi.org/10.5194/nhess-2022-50
Preprint. Discussion started: 11 March 2022

- El Niño Southern Oscillation (ENSO) shows between 5 and 6 years (Stuiver and Braziunas, 1989) although they may be harmonic components of the 11-year sunspot cycle (Lamb, 1972). On the other hand, the warm phase of the ENSO may range between 2 and 7 years (Fleming and Quilty, 2006).
- The North Atlantic Oscillation (NAO) shows cycles of between 6 and 10 years (Hurrell, 1995; Pozo-Vázquez et al., 2000).
- The sunspot cycle (Stuiver and Braziunas, 1989) shows cycles of between 10.5 and 12 years.
- The Hale cycle (Hoyt and Schatten, 1997) has associated cycles of between 20 and 25 years.
- There are other cycles associated to solar activity and lunar tidal cycles, such as 18.6, 26.8 and 47.6 years (Currie et al., 1993; Pardo-Igúzquiza and Rodríguez-Tovar, 2012; Williams, 1981).
- Atlantic Multidecadal Oscillation (Hoeppe, 2016; Wills et al., 2019).

The Spectral analysis estimates the distribution (over frequency) of the power contained in data series (Jenkins and Watts, 1968; Pardo-Igúzquiza and Rodríguez-Tovar, 2012). The presence and statistical significance of natural climate cycles in long-term series in rainfall stations (Karagiannidis et al., 2008; Knippertz, 2003) has been determined by Spectral analysis. The best method to infer the power spectrum is the Blackman–Tukey approach, which offers better results as the climate cycles are well identified and the statistical confidence is higher (Luque-Espinar et al., 2008, 2017; Pardo-Igúzquiza and Rodríguez-Tovar, 2012).

A clear relationship between major landslide events and long-periods of intense rainfall is recorded across the world. In the last hundred years, numerous extraordinary climatic events were described in Spain generating extensive landslide motion (Corominas, 2006). Thus, the definition of the rainfall conditions that, when reached or exceeded, are likely to trigger the failure is very relevant for forecasting rainfall-induced landslides. Abundant literature regarding rainfall thresholds for triggering landslides exists (Schuster and Turner, 1996; Terlien, 1998; Wieczorek and Guzzetti, 2000; Guzzetti et al., 2008; Capparelli and Versace, 2011; ; Staley et al., 2013; Mathew et al., 2014; Huang et al., 2015; ; Piciullo et al., 2017; Melillo et al., 2020;).

In the Majorca site, the island suffered persistent and abnormal precipitations in the period spanning from 2008 to 2010 thattriggered numerous landslides (Mateos et al., 2012). Luque-Espinar et al. (2017) carried out a temporal analysis -by means of spectral techniques- using a set of monthly hydrological and meteorological series of the Serra de Tramuntana mountain of Majorca, where they show the predominant influence of ENSO, NAO and Sunspot in the rainiest periods. They also concluded that the cycle most directly related to the occurrence of landslides of greater magnitude is NAO (7.5y). However, this work focused exclusively on the temporal aspect, but did not analyse the spatial distribution of the climatic cycles, or the spatial distribution of rainfall during dry, medium, and wet years on the island.

Following on from Luque-Espinar et al. (2017), this study takes a broader approach to the influence, not only temporal but also spatial, of climatic cycles. To carry out this work, 62 meteorological stations distributed throughout the island have been selected. Most of the rainfall stations (RS) have had at least daily rainfall data for the last 30 years. Based on this data, a spectral analysis has been carried out, allowing us to identify the natural climate cycles of relevance in Majorca. The statistical confidence values of each climate cycle have been estimated by geostatistical methods to determine the degree to which the

https://doi.org/10.5194/nhess-2022-50
Preprint. Discussion started: 11 March 2022

Natural Hazards and Earth System Sciences
Open Access
Discussions

island of Majorca has been affected. These values have been reclassified from 0 (not detected) to 4 (more than 99% statistical confidence). From the rainfall time series, other variables of interest have been estimated, such as the distribution of rainfall into dry type years (DY), average type years (AY) and wet type years (WY). In addition, several years of the period under study have been selected according to the typology of type years, comparing the rainfall records.

Finally, as an application and validation of the work, we have spatially correlated the sectors of the island of Majorca with the greatest danger of intense rainfall and the inventory of the 423 landslides inventoried in the Serra de Tramuntana of Majorca over the last 30 years.

2 Study area

The island of Majorca is part of the Balearic archipelago, in the western Mediterranean Sea. It has an area of 3677 km^2 and consists of various geomorphological domains, alternating ranges and flat areas (Figure 1). The Tramuntana mountain range, almost 90 km long, forms the NW backbone of the island. It is an Alpine range with a step relief and rises 1,445m a.s.l at Puig Major, , the highest peak on the island .

The climate in Majorca is typically Mediterranean, with mild winters and hot dry summers. The annual average temperature being of 16.6 ºC. The variability of precipitation in Majorca shows values that range from 1400 mm (in the Tramuntana range) to 300 mm in the southern coast (Llucmajor)

Rainfall is often in torrents and it is concentrated into a very few days, with maximum precipitation in 24 h exceeding 300 mm (Mateos et al., 2007). These extreme events preferably take place during the autumn months due to the high sea temperatures during the summer. This phenomenon is known as a DANA (cut-off low). During the spanning period 2008-2010, the island of Majorca suffered from a series of very cold and rainy winters. Rainfall values of up to 296 mm/24h mm were recorded in the central part of the Tramuntana range and the temperatures dropped below 0ºC on numerous occasions, causing extensive frosts in the mountains.. As a result, 66 landslides were triggered, which generated road closures and severe impacts through the Tramuntana range (Mateos et al., 2014).

For the present work, we have updated the landslide inventory in the Tramuntana range. This inventory is part of the landslide database (BD MOVES) of the Geological and Mining Institute of Spain (IGME) and consists of 925 events since the XVIII (BDMoves). Most of the slope movements (76%) are rockfalls, as hard rocks predominate in the range, especially Jurassic limestone and dolostone (Mateos et al., 2016; Sarro et al., 2014). Regarding the last 30 years, the landslide inventory is more complete, incorporating information on the magnitude of the events and their exact location and dating. In this work, we exploit these 30-years (1991-2020) of landslides as they correlate with the minimum rainfall data series. During the past 30 years, 423 events took place in the Tramuntana range; 91% of them were rockfalls, and the rest were earth landslides, complex landslides and debris flows.

https://doi.org/10.5194/nhess-2022-50
Preprint. Discussion started: 11 March 2022

3 Materials and methods

3.1. Spectral analysis

Spectral analysis or harmonic analysis (Bras and Rodríguez-Iturbe, 1993; Jenkins and Watts, 1968; Yevjevich, 1972) is a statistical technique used to identify cyclic components in a time series. The signal component represents the structured part of the time series, made up of a small number of embedded periodicities or cycles repeated over a long time. This information shows a random component or noise that may be white noise, but will more often be red noise. The time series are represented by a finite number of measurements at regular or irregular time intervals. The presence of trends in time series means a cyclic component of a longer period. These trends plus real trends and other factors give rise to noise in the low frequencies or red noise.

In this context, the time series is a linear combination of sinusoidal functions of known periods but of unknown amplitude and phase. The modulus of the amplitude is linked to the variance of the time series and is related to the oscillation at each frequency. The representation of the square of the modulus versus frequency is known as the power spectrum. The indirect method proposed by Blackman & Tukey (1958) has been used due to its being a robust approach which yields good results in this kind of studies (Luque-Espinar et al., 2017, 2008).

The power spectrum (Pardo-Igúzquiza and Rodríguez-Tovar, 2004) is calculated from the covariance function by Eq. (1):

$$\hat{S}(\omega)=\frac{1}{\pi}\left\{\lambda(0)\hat{C}(0)+\sum_{k=1}^{M}\lambda(k)\hat{C}(k)\cos(\omega k)\right\} \tag{1}$$

Where:

$\hat{S}(\omega)$: estimated power spectrum for frequency ω

$\hat{C}(k)$: estimated covariance function for the *k*-th lag

cos(·): cosine

$\lambda(k)$: weighting function, known a lag window, which is used to give less weight to the covariance estimates as the lag increases

For large lags, the estimated covariance function is less reliable. The lag window used was the Tukey window following Eq. (2):

$$\lambda(k)=\frac{1}{2}\left\{1+\cos\left(\frac{\pi k}{M}\right)\right\} \quad 0\le k\le M \tag{2}$$

M means maximum number of lags for the covariance function used in the spectral estimation. N-1 is the maximum number of lags, where N is the number of experimental data. However, with large values for M, a great number of peaks will be seen in the estimated power spectrum, most representing spurious cycles. When M is very small, significant cycles will not be seen

https://doi.org/10.5194/nhess-2022-50
Preprint. Discussion started: 11 March 2022

in the estimated power spectrum. For this reason, we used a value of M = N/2 in order to resolve peaks, and a value of M = N/4 to determine which peaks are the most significant.

Confidence levels were estimated for the inferred power spectrum using a small value for N. The approach of this research consists in fitting a background power spectrum with no cyclic component, but rather a smooth continuous spectrum, which is done by fitting the spectrum of an autoregressive process of order one. We then take into account the known result for the one-sided confidence band of the power spectrum estimator (Eq. 3):

$$\mathrm{P}\left(\upsilon \frac{\hat{S}(\omega)}{S(\omega)} < \chi^2_{\upsilon,\alpha}\right) = 1-\alpha \quad (3)$$

Where

$\mathrm{P}(\cdot)$: probability operator

$\hat{S}(\omega)$: power spectrum estimate for frequency ω

S(ω): underlying power spectrum for frequency ω

υ: number of degrees of freedom. For the Blackman–Tukey estimate with a Tukey lag window, the number of degrees of freedom is *2.67 N/M*

$\chi^2_{\upsilon,\alpha}$: is the α quantile of a Chi-square distribution with υ degrees of freedom

α: significance level

For this study, we established five confidence levels (CL): 0%, <90%, 90%, 95% and 99%.

When cycles are well identified, simulations can be performed to reproduce their behaviour (Luque-Espinar et al., 2017). In this sense, calculating the amplitude and frequency for each cycle is necessary and is added to the most representative cycles.

3.2. Simulations of temporal series

The simulations have been carried out by mean of frequency (F) and power spectrum (S). First, the amplitude is estimated for every cycle using the Eq. 4:

$$P_i = \sigma^2 \frac{S_i}{(S_1 + \cdots + S_n)} \quad (4)$$

Where,

$$A_i = \sqrt{P_i}$$

A_i: cycle amplitude

A point is simulated by the next Eq. 5:

$$G_i = A_i \cos(2\pi t S_i + D) \quad (5)$$

G_i: simulated point for the time t

A_i: cycle amplitude i

cos: cosine

https://doi.org/10.5194/nhess-2022-50
Preprint. Discussion started: 11 March 2022

t: time

S_i: spectral value of the cycle

D: phase shift (radians). Change between 0 and 3.14.

3.3 Geostatistics

Geostatistics (Chiles and Delfiner, 2012; Deutsch and Journel, 1992; Isaaks and Srivastava, 1991) is widely accepted in science as a methodology for solving estimation problems based on the Theory of Regionalised Variables. These variables are distributed in space and show a correlation structure or spatial variability represented by the variogram function representing a structured and a random part (Matheron, 1965). The variogram is an intrinsic random function that represents half of the mean square increments of the spatial variable for distant points, vector h (Eq.6).

$$\gamma(h) = 1/2E\{Z(x) - Z(x+h)\}^2 \qquad (6)$$

The variogram is therefore a vector function that quantifies the variance of the first-order quadratic increments of the function. The variogram allows the spatial variability of the variable to be analysed as a function of distance, thus revealing the structure of variation of the variable. The unbiased estimator of the variogram function is obtained from the data by means of the Eq.7

$$\gamma(h) = \frac{1}{2NP(h)} \sum_{i=1}^{NP(h)} \{z(x_i) - z(x_{i+h})\}^2 \qquad (7)$$

Where $z(x_i)$ and $z(x_{i+h})$ are the observed values of the variable at points x_i and x_{i+h}; $NP(h)$ is the number of distant data pairs h. Once the experimental variogram is computed, a theoretical model is fitted and incorporated into the spatial geostatistical estimation by kriging.

Kriging is the geostatistical estimation method that provides the most probable value of a variable at a non-experimental point. There are several estimation methods adapted to different problems. These methods are classified into two groups according to the structure of the estimator, linear and non-linear. In this work, ordinary kriging (OK) has been chosen as it is better adapted to the problem under study.

3.4. Rainfall data series

We have exploited data series from AEMET (Spanish Meteorological Agen) for 62 meteorological stations distributed through the island and mainly concentrated in the ranges (Llevant, Central and Tramuntana) (Fig 1.). The stations have a minimum of 30 years of daily records, although a significant group exceeds 50 years. 35 (56.5%) of the rain gauges are located in the Tramuntana range, which allows an in-depth analysis of the rainfall data in the most hazardous region for landslides.

The maximum daily rainfall is concentrated in the Serra de la Tramuntana, especially in the municipalities of Bunyola, Escorça and Sóller. The annual rainfall data show very varied standard values, as do the daily records, although they essentially follow very similar spatial patterns and are conditioned by the topography of the island. From the meteorological series, the standard years of each meteorological series have been estimated (Table 1). The dry type year (DY) represents the mean value of the lower quartile of each rainfall series, the average type year (AY) represents the mean value of the entire rainfall record of each

https://doi.org/10.5194/nhess-2022-50
Preprint. Discussion started: 11 March 2022

Natural Hazards and Earth System Sciences Discussions

series and the wet type year (WY) represents the mean value of the upper quartile of each rainfall series. In addition, the analysis of the rainfall series studied has made it possible to identify a series of years in which the stations have rainfall values similar to the estimated type years (Table 1). In this sense, the years 1983 and 1999 were very dry; the years 1985 and 2003 show values similar to those of the average year; and finally, the years 1972 and 2008 were wet years.

3.5. Landslide inventory

During the past 30 years, 423 landslide events were registered, mostly rockfalls (385 events). Figure 2 shows the temporal distribution of the landslide events, the year 2016 standing out with 60 landslides. Most of these records were provided by the Road Maintenance Service of Majorca and are related to small rockfalls (< 100 m^3) with source areas located in the road-cuttings. If we only consider the magnitude of the rockfalls in natural slopes, 3 of the largest ones took place during the rainy period 2008-2010 (Fig. 2). Table 2 shows the main parameters of the 5 largest, natural rockfalls inventoried and dated during the spanning period 1991-2020. The largest one took place on the night of 19th December 2008. The Son Cocó rock avalanche (Alaró) -with a length of 650 m- destroyed the pine wood in its path, leaving a tongue of blocks over an area of 60000 m^2 and 300000 m^3 in volume (Fig. 2). Some of the blocks have a volume of over 1500 m^3 and are several tons in weight.

4. Results

4.1. Spectral analysis

The rainfall in Majorca shows an irregular spatial distribution, especially in the Tramuntana range. The topography of this range imposes the climatic variations typical of mountainous regions: higher elevations, and heavy precipitation (Mateos et al., 2007).

The highest values of statistical confidence estimated in the climate cycles correspond to 5.6y (ENSO), 7.5y (NAO), 3.5y (ENSO), QBO and 6.4y (ENSO/NAO).

Figure 3 shows some representative rainfall records for the island of Majorca and the results of the spectral analysis.

The rainfall gauge analysed shows a multitude of climatic cycles with different statistical significance, reflecting the complexity of Majorca's climate. Figure 4 shows the main cycles estimated according to the number of detections and the highest statistical confidence values determined.

4.2. Spatial estimation of the influence of climatic cycles

The results of the spectral analysis have made it possible to identify the climatic cycles with the most influence on rainfall on the island of Majorca. The statistical confidence values estimated at each rainfall station have been reclassified from 0 (not detected) to 4 (more than 99% statistical confidence) and have been estimated using geostatistical methods to determine the degree of influence of each climatic cycle (Figure 5). However, when there are a significant number of stations where the cycle

https://doi.org/10.5194/nhess-2022-50
Preprint. Discussion started: 11 March 2022

Natural Hazards and Earth System Sciences
Open Access
EGU
Discussions

has not been detected, a dichotomous transformation has been chosen, i.e. observed (1), not observed (0), as in the case of ENSO (6.4y) and Sunspot (11.2y).

It should be noted that the experimental variograms obtained show great continuity, reflecting a well-correlated variable in space. This has allowed a good fit in all cases to a spherical variogram model, with a nugget effect in all cases (less than 25% of sill) and well-defined sills. The southern part of the island, due to the smaller number of meteorological stations, has offered small uncertainties in the estimation, which is why some estimated cycles show discontinuities in the mapping, as is the case with ENSO 5.6y and Sunspot 11.2y.

In general, most of the mapped cycles affect the whole island (Figure 5), except for the 6.4y (ENSO/NAO) and 11.2y (Sunspot) cycles which, in some meteorological series, have not been detected with sufficient clarity. According to the results obtained, the ENSO cycle (5.6y) influences the whole island, although the highest values are concentrated in sectors of the south coast, in the municipalities of Campos, Santanyí and Ses Salines; and in municipalities located in the Tramuntana range, such as Escorça, Campanet, Bunyola, Santa Maria del Camí, Valldemossa or Andratx. The NAO cycle (7.5y) presents the highest values distributed in different parts of the island, especially in relation to the Tramuntana range (municipalities of Palma, Marratxí, Bunyola and Esporles), southern coastal areas (Ses Salines, Campos and Santanyí) and the eastern coast (San Serverva and Sant Llorenç). The ENSO cycle (3.5y) particularly affects a strip of municipalities located to the south of the Tramuntana, between the municipalities of Sencelles and Inca up to Alcúdia. However, it should also be taken into account that the lowest value of this cycle is close to 2, i.e. probabilities greater than 90%. The QBO cycle shows the highest values of statistical significance on the west coast, in the municipalities of Fornalutx, Escorça, Sóller, Bunyola, Campanet and Pollença. The highest probabilities of the influence of the 6.4y cycle (ENSO/NAO) are to be found in some municipalities on the south and east coast of the island, mainly Llucmajor, Manacor, Felanitx and Santanyí. The Sunspot cycle is more likely to affect sectors linked to the west and north coast of the island, especially the municipalities of Banyalbufar, Puigpunyent, Esporles, Valldemossa, Escorça, Pollensa and Artá. Finally, the HALO cycle is most significant in Santa María del Camí, Marratxi, Palma, Escorça, Pollença, Buyonla, Alaro, Sóller and Consell.

Overall, the NW of the island is where the highest statistical confidence values are concentrated for all the above-mentioned cycles and some sectors of the east coast. The central area of the Serra de Tramuntana, Bunyola-Fornalutx-Escorça-Sóller, stands out, with high statistical confidence values in practically all the cycles.

Regarding the location of the 5 largest rockfalls (Table 2) on the statistical confidence maps of the climate cycles, all of which include one or more of the detachments in the areas of greatest significance, with NAO (7.5 y), QBO and HALO (22.4 y) – as well as, to a lesser extent, Sunspot - being the best fit.

4.3. Spatial analysis of typical years

To complement the spectral analysis, the daily rainfall data have been transformed into annual data to study the spatio-temporal behaviour of rainfall in an average, wet and dry type year. A selection has also been made of a series of years whose stations present values that are very similar or equal to the estimated type years.

https://doi.org/10.5194/nhess-2022-50
Preprint. Discussion started: 11 March 2022

Figure 6 shows the variogram models fitted to the calculated model years and the selected years. In all cases, the theoretical variogram fitted has been a spherical model, with a similar nugget effect and similar range. This behaviour of the variograms is known as the Proportional Effect and indicates that the variable behaves in space and time in the same way, i.e. it presents the same spatial variability model. Overall, the value of the nugget effect is low in percentage terms, indicating that the variable is very continuous at the origin despite the fact that in some areas of the island the number of rainfall stations is lower. The only difference is the value of the sill, whose value coincides with the variance of the data. This behaviour is potentially of great interest for developing predictive rainfall models for different climate change scenarios, whether or not the spatial behaviour of the rainfall variable defined by the variograms changes.

As an example of the estimation of the type years and selected years, Figure 7 shows the spatial estimation of the wet type year and the year 2008, the wettest of the years studied. The estimates have been made from the fitted variogram models (Figure 6).

From the spatial point of view, the estimation of rainfall according to the fitted variogram models shows a very similar distribution in space and is always strongly influenced by the Tramuntana range, where the maximum values can be seen in all studied cases, especially in the areas oriented to the north and northwest and towards the coast as a whole. On the other hand, the minimum values are located towards the south of the island.

One should also note the great coincidence between the sector where the maximum rainfall is concentrated and the area of maximum probabilities of the main climatic cycles affecting the island. In this sense, if we look at Figure 7 (maximum rainfall) and compare it with Figures 5a, 5b, 5d, 5f and 5g, a significant part of the maximum probabilities of occurrence of these cycles coincides with the area of maximum rainfall recorded on the island. The rest of the cycles show a lower percentage of coincidence.

The superimposition of the five major landslides on figures 7a and 7b shows a very good spatial correlation between the location of these landslides and the areas of highest rainfall in the typical wet year and in 2008. It coincides with the NE sector of the Serra de Tramuntana, where the relief is more pronounced. Specifically, the Son Cocó and Gorg Blau landslides (Fig. 2) took place in December 2008, the latter being located exactly in the core of the wettest sector.

5. Conclusions

The spectral analysis has made it possible to identify the climatic cycles that determine the behaviour of rainfall on the island of Majorca. The lower frequency cycles (>30y) offer doubts regarding the real influence on all the stations, as the historical records are not sufficiently extensive.

This work confirms and improves the results obtained by Luque-Espinar et al. (2017). The intense precipitation that triggers landslides in the Serra de Tramuntana is linked to ENSO and NAO cycles, together with Sunspot and HALO. An important novelty in this work is the influence exerted by QBO, whose spatial estimation of statistical confidence shows the highest values in the areas where the 5 largest landslides are located.

The cycles with the greatest influence on the pluviometry of the study area, from the point of view of statistical confidence, are: 5.6y (ENSO), 7.5y (NAO), 3.5y (ENSO), QBO and, with less weight, 6.4y (ENSO/NAO) and 4.5y (ENSO).

The reclassification of the results of the spectral analysis has made it possible to map the influence of climatic cycles in Majorca using geostatistical methods. The variogram models adjusted to the statistical confidence variable reflect a very continuous behaviour in space, which has made it possible to generate cartographies that clearly show the different climatic influences in the working area.

The sectors where the maximum rainfall is concentrated show a variable degree of coincidence with the maximum values of statistical confidence of the climatic cycles that most influence the island. In this sense, the highest coincidence, in decreasing order, is QBO, NAO 7.5y, Sunspot, HALO, ENSO 5.6y, ENSO 3.5y and ENSO/NAO 6.4y.

The spatial variability of rainfall represented by the variograms and the presence of a proportional effect in the variograms indicate that the spatial behaviour of the variable is independent on the amount of rainfall.

The Serra de Tramuntana, to the NW of the island, is not only the rainiest region of the island, but also the area where the highest values of statistical confidence for the set of climatic cycles are concentrated. In this region 423 landslides have been inventoried in the last 30 years. The five landslides with the highest magnitude in the series are located in the areas with the highest statistical confidence.

The methodology presented in this work is applicable to any case study that has sufficient meteorological stations and historical rainfall records, and can be related to other geological hazards linked to water, such as floods. In this sense, this type of analysis offers a calibrated and validated instrument to the institutions responsible for emergency management, which can be extremely useful for decision-making in the face of this type of geological hazard.

Acknowledgements

This work has been developed in the framework of the RISKCOAST project (Ref: SOE3/P4/E0868) funded by the Interreg SUDOE programme (3rd call for proposals). Many thanks to AEMET (the Spanish Meteorological Agency) for the rainfall data as well as to the Road Maintenance Service of Majorca and the Emergency Service of the Balearic Islands for providing many landslide events.

References

Capparelli, G. and Versace, P.: FLaIR and SUSHI: two mathematical models for early warning of landslides induced by rainfall, Landslides, 8, 67–79, https://doi.org/10.1007/s10346-010-0228-6, 2011.

Corominas, J.: El clima y sus consequencias sobre la actividad de los movimientos de ladera en España, 89–113, 2006.

Currie, R. G., Wyatt, T., and O'Brien, D. P.: Deterministic signals in European fish catches, wine harvests, and sea-level, and further experiments, 13, 665–687, https://doi.org/10.1002/joc.3370130607, 1993.

https://doi.org/10.5194/nhess-2022-50
Preprint. Discussion started: 11 March 2022

Fleming, S. W. and Quilty, E. J.: Aquifer Responses to El Niño–Southern Oscillation, Southwest British Columbia, 44, 595–599, https://doi.org/10.1111/j.1745-6584.2006.00187.x, 2006.

.

Guzzetti, F., Peruccacci, S., Rossi, M., and Stark, C. P.: The rainfall intensity–duration control of shallow landslides and debris flows: an update, Landslides, 5, 3–17, https://doi.org/10.1007/s10346-007-0112-1, 2008.

Hoeppe, P.: Trends in weather related disasters – Consequences for insurers and society, Weather and Climate Extremes, 11, 70–79, https://doi.org/10.1016/j.wace.2015.10.002, 2016.

Hoyt, D. V. and Schatten, K. H.: The Role of the Sun in Climate Change, Oxford University Press, 288 pp., 1997.

Huang, J., Ju, N. P., Liao, Y. J., and Liu, D. D.: Determination of rainfall thresholds for shallow landslides by a probabilistic and empirical method, 15, 2715–2723, https://doi.org/10.5194/nhess-15-2715-2015, 2015.

Hurrell, J. W.: Decadal Trends in the North Atlantic Oscillation: Regional Temperatures and Precipitation, https://doi.org/10.1126/science.269.5224.676, 1995.

BDMoves: http://info.igme.es/BD2DMoves/).

Jenkins, G. M. and Watts, D. G.: Spectral analysis and its applications, Holden-Day, San Francisco, 525 pp., 1968.

Karagiannidis, A. F., Bloutsos, A. A., Maheras, P., and Sachsamanoglou, Ch.: Some statistical characteristics of precipitation in Europe, 91, 193–204, https://doi.org/10.1007/s00704-007-0303-7, 2008.

Knippertz, P.: Tropical–Extratropical Interactions Causing Precipitation in Northwest Africa: Statistical Analysis and Seasonal Variations, 131, 3069–3076, https://doi.org/10.1175/1520-0493(2003)131<3069:TICPIN>2.0.CO;2, 2003.

Labitzke, K., van Loon, H., Shine, K., Pecker, J.-C., and Runcorn, S. K.: Associations between the 11-year solar cycle, the quasi-biennial oscillation and the atmosphere: a summary of recent work, 330, 577–589, https://doi.org/10.1098/rsta.1990.0039, 1990.

Lamb, H. H.: Climate: present, past and future, Methuen, London New York, 1972.

Luque-Espinar, J. A., Chica-Olmo, M., Pardo-Igúzquiza, E., and García-Soldado, M. J.: Influence of climatological cycles on hydraulic heads across a Spanish aquifer, Journal of Hydrology, 354, 33–52, https://doi.org/10.1016/j.jhydrol.2008.02.014, 2008.

Luque-Espinar, J. A., Mateos, R. M., García-Moreno, I., Pardo-Igúzquiza, E., and Herrera, G.: Spectral analysis of climate cycles to predict rainfall induced landslides in the western Mediterranean (Majorca, Spain), Nat Hazards, 89, 985–1007, https://doi.org/10.1007/s11069-017-3003-3, 2017.

Mateos, R. M., Azañón, J. M., and Morales, R.: Regional prediction of landslides in the Tramuntana Range (Majorca) using probability analysis of intense rainfall, 287–306, https://doi.org/10.1127/0372-8854/2007/0051-0287, 2007.

Mateos, R. M., García-Moreno, I., and Azañón, J. M.: Freeze–thaw cycles and rainfall as triggering factors of mass movements in a warm Mediterranean region: the case of the Tramuntana Range (Majorca, Spain), Landslides, 9, 417–432, https://doi.org/10.1007/s10346-011-0290-8, 2012.

https://doi.org/10.5194/nhess-2022-50
Preprint. Discussion started: 11 March 2022

Mateos, R. M., Garcia, I., Reichenbach, P., Herrera, G., Rius, J., Aguilo, R., and Roldan, F. J.: Seasonal rockfall risk assessment along transportation network: a sample from Mallorca (Spain), 5467, 2014.

Mateos, R. M., García-Moreno, I., Reichenbach, P., Herrera, G., Sarro, R., Rius, J., Aguiló, R., and Fiorucci, F.: Calibration and validation of rockfall modelling at regional scale: application along a roadway in Mallorca (Spain) and organization of its management, 13, 751–763, https://doi.org/10.1007/s10346-015-0602-5, 2016.

Mathew, J., Babu, D. G., Kundu, S., Kumar, K. V., and Pant, C. C.: Integrating intensity–duration-based rainfall threshold and antecedent rainfall-based probability estimate towards generating early warning for rainfall-induced landslides in parts of the Garhwal Himalaya, India, Landslides, 11, 575–588, https://doi.org/10.1007/s10346-013-0408-2, 2014.

Melillo, M., Gariano, S. L., Peruccacci, S., Sarro, R., Mateos, R. M., and Brunetti, M. T.: Rainfall and rockfalls in the Canary Islands: assessing a seasonal link, 1–26, https://doi.org/10.5194/nhess-2020-111, 2020.

Muñoz-Díaz, D. and Rodrigo, F. S.: Influence of the El Niño-Southern Oscillation on the probability of dry and wet seasons in Spain, 30, 1–12, 2005.

Pardo-Igúzquiza, E. and Rodríguez-Tovar, F. J.: Spectral and cross-spectral analysis of uneven time series with the smoothed Lomb–Scargle periodogram and Monte Carlo evaluation of statistical significance, Computers & Geosciences, 49, 207–216, https://doi.org/10.1016/j.cageo.2012.06.018, 2012.

Piciullo, L., Gariano, S. L., Melillo, M., Brunetti, M. T., Peruccacci, S., Guzzetti, F., and Calvello, M.: Definition and performance of a threshold-based regional early warning model for rainfall-induced landslides, Landslides, 14, 995–1008, https://doi.org/10.1007/s10346-016-0750-2, 2017.

Pozo-Vázquez, D., Esteban-Parra, M. j., Rodrigo, F. s., and Castro-Díez, Y.: An analysis of the variability of the North Atlantic Oscillation in the time and the frequency domains, 20, 1675–1692, https://doi.org/10.1002/1097-0088(20001130)20:14<1675::AID-JOC564>3.0.CO;2-C, 2000.

Rodó, X., Baert, E., and Comín, F. A.: Variations in seasonal rainfall in Southern Europe during the present century: relationships with the North Atlantic Oscillation and the El Niño-Southern Oscillation, Climate Dynamics, 13, 275–284, https://doi.org/10.1007/s003820050165, 1997.

Sarro, R., Mateos, R. M., García-Moreno, I., Herrera, G., Reichenbach, P., Laín, L., and Paredes, C.: The Son Poc rockfall (Mallorca, Spain) on the 6th of March 2013: 3D simulation, 11, 493–503, https://doi.org/10.1007/s10346-014-0487-8, 2014.

Schuster, R. L. and Turner, A. K.: Landslides: investigation and mitigation, National academy Press, Washington, 1996.

Staley, D. M., Kean, J. W., Cannon, S. H., Schmidt, K. M., and Laber, J. L.: Objective definition of rainfall intensity–duration thresholds for the initiation of post-fire debris flows in southern California, Landslides, 10, 547–562, https://doi.org/10.1007/s10346-012-0341-9, 2013.

Stuiver, M. and Braziunas, T.: Atmospheric 14C and century-scale solar oscillations, https://doi.org/10.1038/338405A0, 1989.

Terlien, M. T. J.: The determination of statistical and deterministic hydrological landslide-triggering thresholds, Environmental Geology, 35, 124–130, https://doi.org/10.1007/s002540050299, 1998.

Tramblay, Y., El Adlouni, S., and Servat, E.: Trends and variability in extreme precipitation indices over Maghreb countries, 13, 3235–3248, https://doi.org/10.5194/nhess-13-3235-2013, 2013.

https://doi.org/10.5194/nhess-2022-50
Preprint. Discussion started: 11 March 2022

Wieczorek, G. F. and Guzzetti, F.: A review of rainfall thresholds tor triggering landslides, 2000.

Williams, G. E.: Sunspot periods in the late Precambrian glacial climate and solar–planetary relations, 291, 624–628, https://doi.org/10.1038/291624a0, 1981.

Wills, R. C. J., Armour, K. C., Battisti, D. S., and Hartmann, D. L.: Ocean–Atmosphere Dynamical Coupling Fundamental to the Atlantic Multidecadal Oscillation, 32, 251–272, https://doi.org/10.1175/JCLI-D-18-0269.1, 2019.

Xoplaki, E., Trigo, R. M., García-Herrera, R., Barriopedro, D., D'Andrea, F., Fischer, E. M., Gimeno, L., Gouveia, C., Hernández, E., Kuglitsch, F. G., Mariotti, A., Nieto, R., Pinto, J. G., Pozo-Vázquez, D., Saaroni, H., Toreti, A., Trigo, I. F., Vicente-Serrano, S. M., Yiou, P., and Ziv, B.: Large-Scale Atmospheric Circulation Driving Extreme Climate Events in the Mediterranean and its Related Impacts, in: The Climate of the Mediterranean Region, edited by: Lionello, P., Elsevier, Oxford, 347–417, https://doi.org/10.1016/B978-0-12-416042-2.00006-9, 2012.

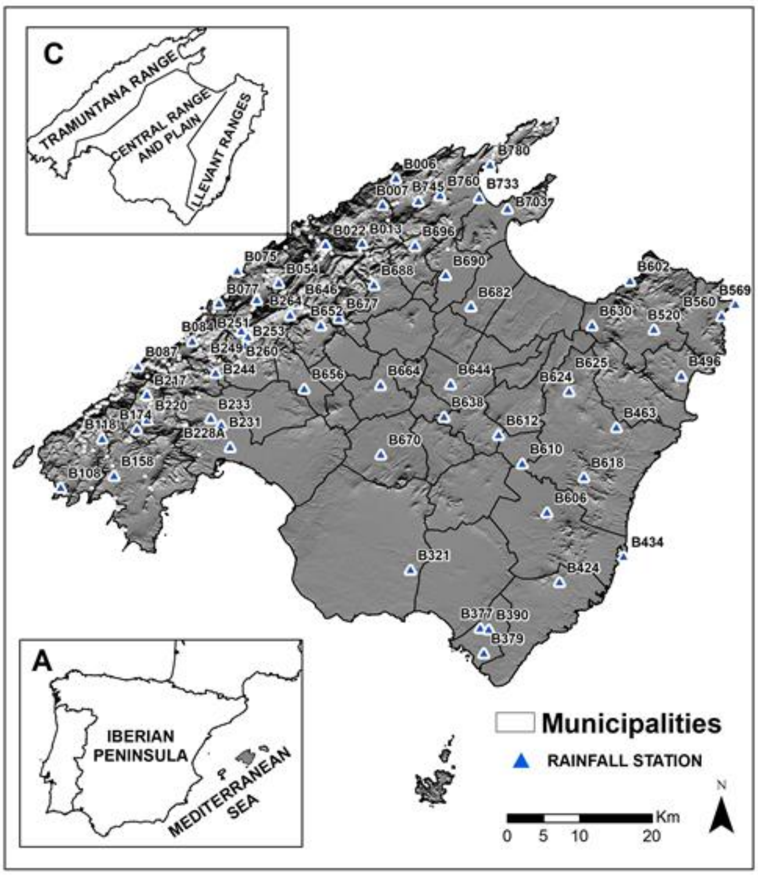

Natural Hazards and Earth System Sciences
Open Access
EGU
Discussions

Figure 1: (A) Location of Majorca in the western Mediterranean. (B) Rainfall stations used in the present work. (C) The main geomorphological domains on the island, highlighting the Tramuntana range in the northern part.

Dry year | Average year | Wet year

Type	473	269	862	Type	662	382	1223	Type	1068	605	2008
Year	Mean	Min	Max	Year	Mean	Min	Max	Year	Mean	Min	Max
1983	347	126	667	1985	670	357	1500	1972	994	536	1725
1999	373	167	756	2003	708	343	1333	2008	896	474	1885

Table 1: Estimated statistic values of the estimated type years and selected natural hydrological years.

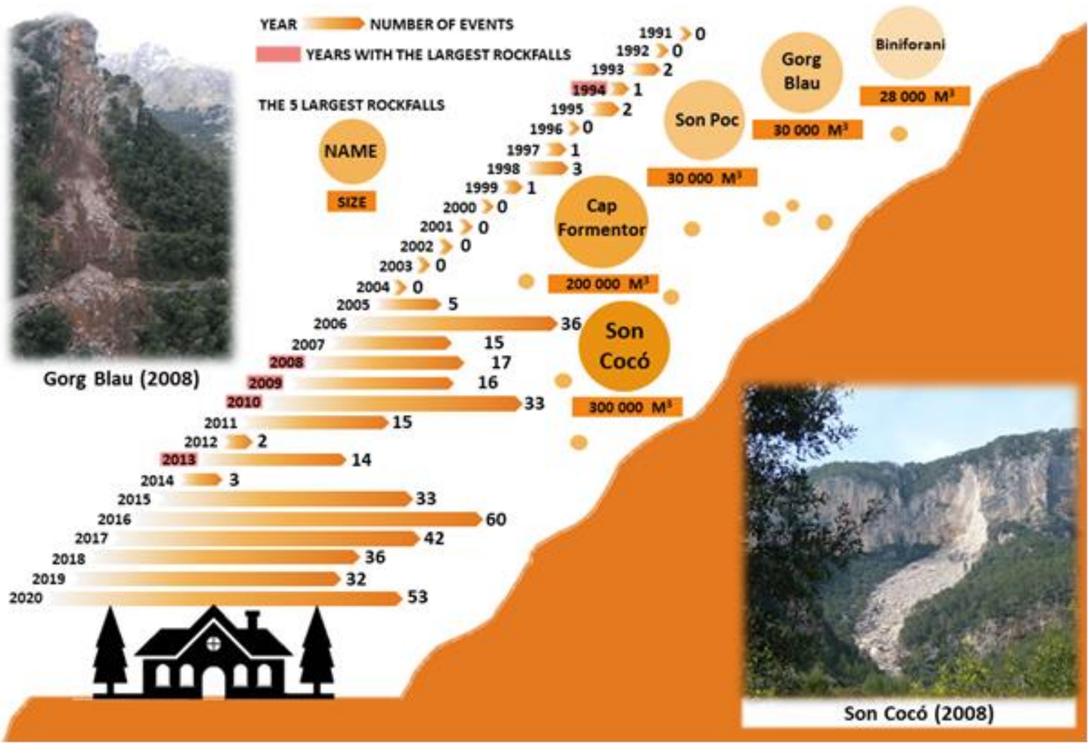

Figure 2: Distribution of the 423 landslide events registered during the past 30 years (1991-2020) in the Tramuntana range of Majorca and the temporal location of the 5 largest (> 28000 m3) and natural-slope rockfalls. There are no records for the first 2 years. Photos of 2 of the largest rockfalls that took place during the rainy, cold period 2008-2010. Right: the Son Cocó rock avalanche in December 2008, the largest rockfall (300000 m3). Left: the Gorg Blau rockfall (30000 m3), also in December 2008. This rockfall cut off the main road of the Tramuntana range during 3.5 months, with repairing costs of over 2.5 M€ (Mateos et al., 2014).

Landslide name	Cap Formentor	Son Cocó	Gorg Blau	Biniforani	Son Poc
Type	Rockfall	Rock avalanche	Rockfall	Rockfall	Rockfall
Municipality	Pollença	Alaró	Escorca	Bunyola	Bunyola
Date	September 1994	19/12/2008	31/12/2008	05/01/2009	06/03/2013
Volume (m^3)	200000	300000	30000	28000	30000
Damage	1 fatality, the Ma-2210 road	Land	Ma-10 road	Land	3 houses

Table 2: The 5 largest, natural-slope rockfalls registered during the past 30 years; 3 of them occurred during the rainy, cold period spanning from 2008 to 2010.

https://doi.org/10.5194/nhess-2022-50
Preprint. Discussion started: 11 March 2022

Natural Hazards and Earth System Sciences
Open Access
EGU
Discussions

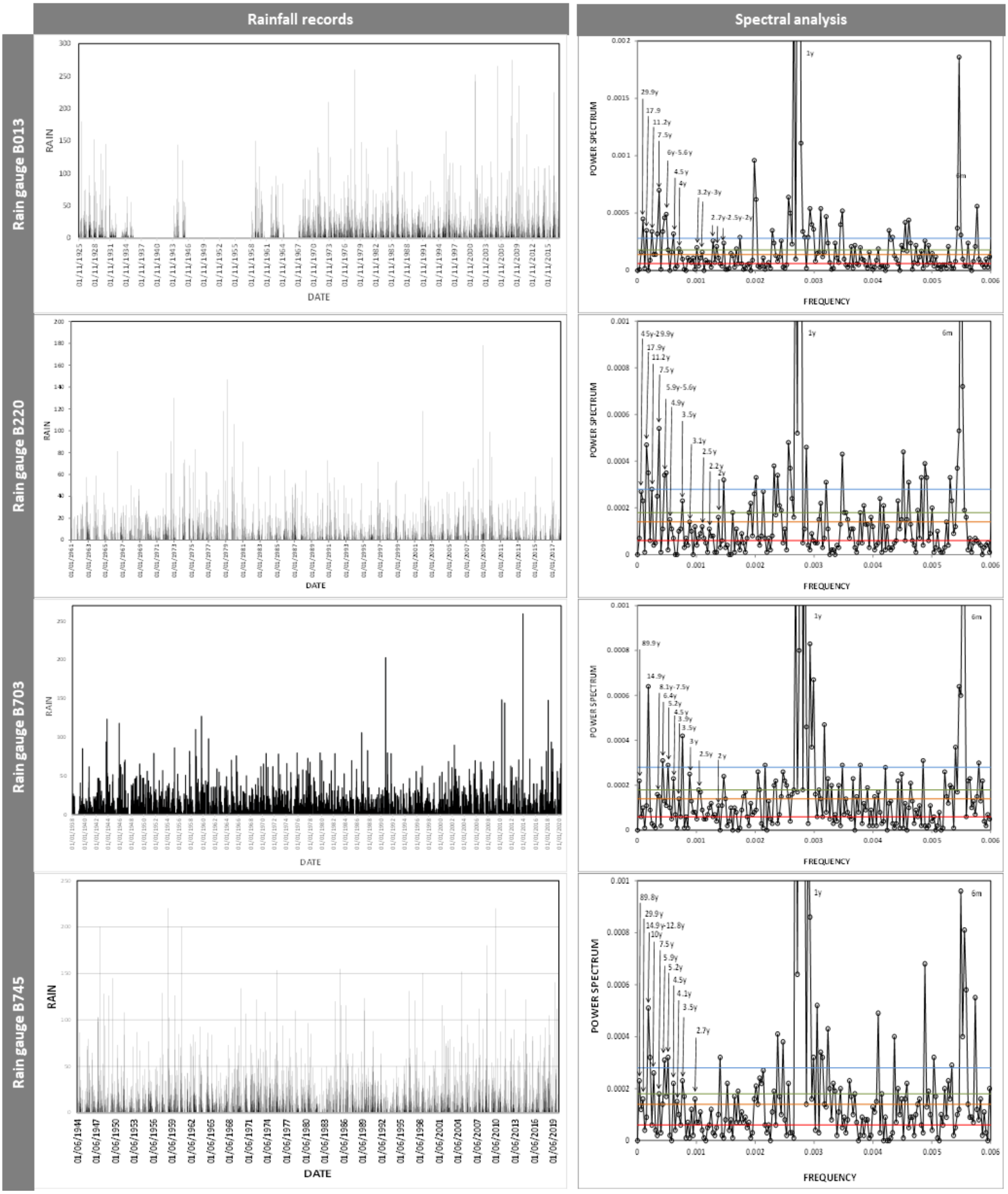

Figure 3: Rainfall records and results of the spectral analysis.

https://doi.org/10.5194/nhess-2022-50
Preprint. Discussion started: 11 March 2022

Natural Hazards and Earth System Sciences
Open Access
Discussions
EGU

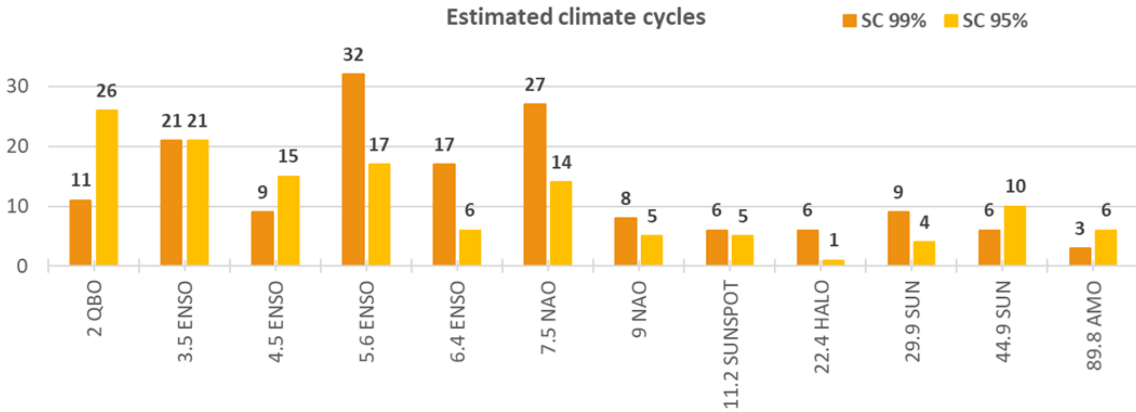

Figure 4: Main estimated climate cycles and statistical confidence values.

https://doi.org/10.5194/nhess-2022-50
Preprint. Discussion started: 11 March 2022

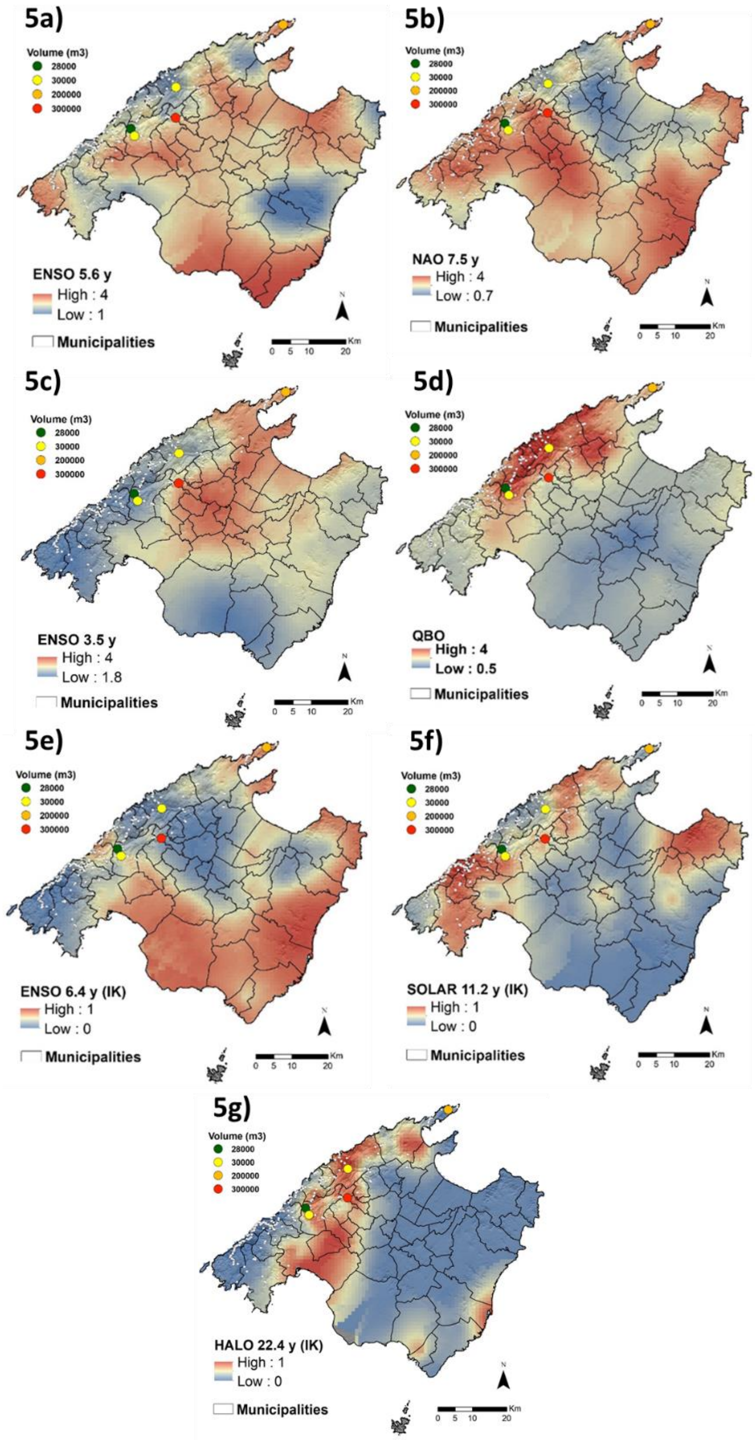

Figure 5: Spatial estimation of the statistical confidence of the climatic cycles with the greatest influence on the island of Majorca using geostatistical methods. The 5 largest rockfalls are located, classified by volume.

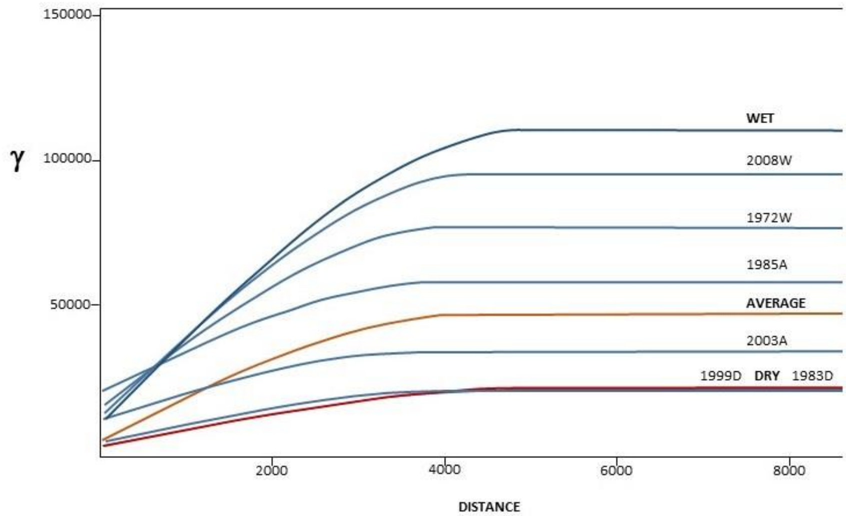

Figure 6: Theoretical variograms fitted for each of the dates selected for the spatial estimation of precipitation.

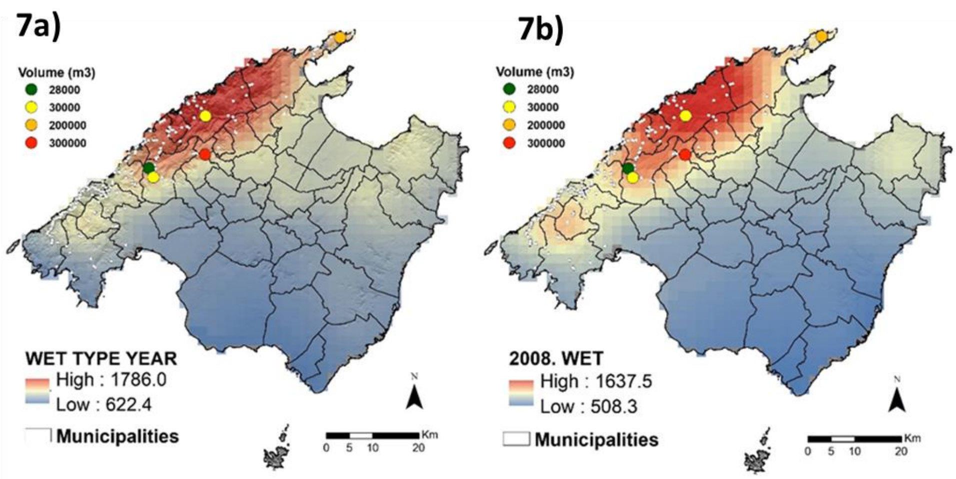

Figure 7: Estimated rainfall in mm in a wet type year, and the year 2008 with similar values to those of the wet type year. The 5 largest rockfalls are located and classified by volume.